Analyzing Production Rate and Carbon Utilization Tradeoffs in CO_2RR Electrolyzers

Steven A. Hawks[a], Victoria M. Ehlinger[b], Thomas Moore[b], Victor A. Beck[b], Adam Z. Weber[c], and Sarah E. Baker[a]**

[a]Materials Science Division, Lawrence Livermore National Laboratory, Livermore, CA 94550, USA.

[b]Computational Engineering Division, Lawrence Livermore National Laboratory, Livermore, CA 94550, USA

[c]Energy Storage and Distributed Resources Division, Lawrence Berkeley National Laboratory, Berkeley, CA 94720

Corresponding Authors
*hawks3@llnl.gov; baker74@llnl.gov

ABSTRACT

Carbon utilization is a crucially important performance characteristic of CO_2 electrolyzers; however, the application of simple and accurate descriptive models to experimental data on this topic are currently lacking. Here, we apply a simple analytical reactor model to parameterize single-pass conversion as a function of feed-gas flow rate and show that it captures a wide body of experimental data in the literature exceptionally well. In doing so, we demonstrate that this simple conceptual approach can characterize progress and capture recent innovations in reactor design. To validate the extracted parameters, we employ a well-established comprehensive model to confirm that the results agree with physical expectations. Finally, we explore the implications of the descriptive model by examining the inherent tradeoff between single-pass conversion

efficiency and reactor productivity. Understanding such tradeoffs is crucially important for advancing this electrolyzer technology toward commercial applications.

TOC GRAPHICS

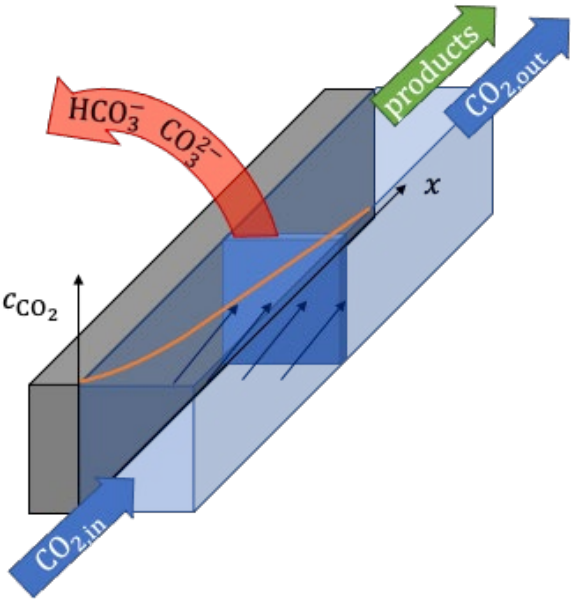

The idea of using electrolyzers to transform CO_2 into value-added products has gained significant attention over the past decade.[1-13] The overall viability of this approach compared to alternative CO_2 mitigation strategies will depend on the confluence of reactor performance and numerous external economic factors.[12, 14-20] When assessing reactor performance, a number of key performance indicators (KPIs) are crucial to consider when evaluating progress. For example, some of these KPIs include system-level characteristics such as specific energy consumption (e.g., kWh/kg product), productivity (e.g., kg product/time/system size or partial current density), and carbon utilization (e.g., single-pass CO_2 conversion efficiency). Most importantly, one must consider these KPIs simultaneously rather than individually as there can be inherent tradeoffs between them. Only by taking a multifaceted approach to performance evaluation can meaningful progress be made across different electrolyzer designs and operation modes. For example, Kungas[21] compared low- and high-temperature electrolysis technologies for producing CO from CO_2 by examining specific energy consumption in kWh/Nm^3 as a function of CO partial current density, which is directly proportional to reactor productivity. For the data considered, the investigation revealed that high-temperature solid-oxide electrolysis had substantially lower specific-energy consumption at a given productivity compared to the low-temperature devices. This example highlights the power of using KPI tradeoff curves to compare reactor designs even when the reactors themselves are radically different. Because high-fidelity tradeoff curves are experimentally laborious to create, it is beneficial to have a simple descriptive model to provide some guidance and insight into why the tradeoff trends as it does, what effective parameters influence the tradeoff, and what the reasonable limits might be given the current design.[22]

Along these lines, here we employ a simple model to understand carbon utilization in CO_2 electrolyzers, enabling an exploration of the relationship between two KPIs: carbon utilization and

reactor productivity. Productivity is important because it is directly tied to capital intensity for a given product output, while single-pass conversion efficiency is important because of the need to efficiently transform CO_2 into products while minimizing downstream separation costs.[16, 17, 20, 23] Previously, Weng et al.[24, 25] developed and examined both gas diffusion electrode (GDE) with liquid electrolyte and membrane-electrode-assembly (MEA)-specific frameworks for modeling CO_2 electrolyzers and used it to examine the conversion and consumption of CO_2 as a function of applied current density. Subsequently, Kas et al.[26] developed a 2-D model for investigating how gradients along the gas channel impact CO_2 conversion and consumption. Experimentally, several studies have focused on single-pass conversion,[27-30] while the Seger group has extensively examined the overall carbon balance within different reactor configurations.[31-34] To the best of our knowledge, though, there has been little work merging models with experimental data on the topic of single-pass conversion efficiency. In fact, CO_2 conversion efficiency in general has received relatively little attention despite its importance in CO_2 electrolyzers.

Here, we establish a model that describes experimental data across several different reactor designs from different research groups. We model the gas channel as a simple plug-flow reactor (PFR), which we find accurately characterizes a wide cross section of CO_2 conversion results in the literature for GDE and MEA-type devices.[28, 35-37] We further link our simplified PFR model to the more comprehensive model of Weng et al.[24, 25] to compare how the PFR parameters correlate with a more physically detailed model. With the foundation for single-pass conversion efficiency firmly established, we then examine the compromise between productivity and conversion efficiency as a function of CO_2 feed rate. Our results have strong implications for reactor control and operation as well as the optimization of reactor design. This work can serve as motivation for exploring new approaches to CO_2 electrolyzers and can aide in understanding the ultimate

capabilities of CO_2 electrolysis. Finally, we hope that this analysis serves to encourage the development of system-level KPIs that allow for better comparison of different electrolyzer designs.

For a simple descriptive model of single-pass conversion, we envision a generic reactor structure like that depicted in **Fig. 1**. For our purposes, the details of the anode, cathode, and separator structures are not relevant, as the reactor is simply imagined as a CO_2 sink attached to a gas channel.

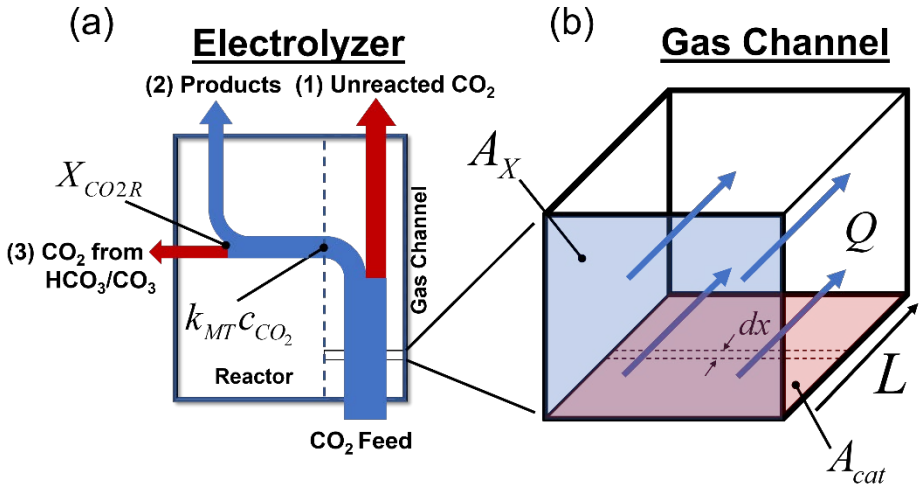

Fig. 1 (a) Overview of model concepts, highlighting the three different paths that influent CO_2 is imagined taking through the electrolyzer. (b) Conceptual representation of a portion of the gas channel.

With this in mind, **Fig. 1a** sketches the three distinct pathways that we consider for CO_2 passing through the reactor. These pathways include: 1.) incoming CO_2 passing directly through the gas channel without being reacted, 2.) incoming CO_2 that enters the reactor and is electrochemically reduced, and 3.) incoming CO_2 that enters the reactor but reacts with hydroxide to form (bi)carbonate. We aim to capture these effects by considering the gas channel as a PFR-like sub-

reactor within the system. To this end, if the underlying electrochemical assembly acts as an irreversible first-order sink, then standard PFR analysis predicts that

$$X_{CO_2} = X_{CO_2R}\left(1 - e^{-\frac{k_{MT}A_{cat}}{Q}}\right) \quad (1)$$

where X_{CO_2} is the single-pass CO_2 conversion efficiency, X_{CO_2R} is the internal CO_2 conversion efficiency, Q is taken here as the total volumetric flow rate into the reactor (cm^3/s), k_{MT} is the effective overall effective mass-transfer coefficient for the electrolyzer (cm/s), and A_{cat} (**Fig. 1b**) is the geometric area of catalyst that interfaces the gas channel (cm^2). We define single-pass conversion efficiency X_{CO_2} (sometimes referred to as simply CO_2 conversion or CO_2 utilization) as the ratio of CO_2 molecules electrochemically reduced per unit time divided by the total number of CO_2 molecules fed into the gas channel per unit time, while the internal CO_2 conversion efficiency X_{CO_2R} is defined as the ratio of CO_2 molecules electrochemically reduced per unit time to the total CO_2 molecules that enter the porous electrode from the gas channel per unit time, **Fig. 1a.** We note here that the ratio X_{CO_2} / X_{CO_2R} is equal to the ratio of the total CO_2 consumption of the reactor (CO_2R + bicarbonate formation) to the total CO_2 fed to the gas channel and that the term $k_{MT}A_{cat} / Q$ is the Damköhler number (Da) for a PFR with first-order kinetics. While Eqn. (1) can be found in chemical engineering textbooks, such as Levenspiel and Fogler,[38, 39] we also provide a detailed derivation in the supporting information (SI).

There are several crucial assumptions in using Eqn. (1) that must be discussed. First, by using Eqn. (1), we ignore gas gradients across the cross-section (A_X in **Fig. 1b**) of the gas channel and only consider changes along the channel length (i.e., gas flow direction). Second, we ignore any gas-phase interactions and assume that the underlying reactor behaves as a simple first-order

sink for CO_2 from the gas channel, which is likely a reasonable assumption since CO_2 dissolution, the first electron transfer in CO_2R, and the reaction between CO_2 and hydroxide to form bicarbonate are all first order. To further justify this assumption, though, we fit a subset of the data below to an arbitrary reaction order and find that the effective reaction order is close to unity with good confidence (see **Fig. S1** in the SI). Third, we ignore diffusion and flow dispersion along the flow direction of the channel, only accounting for the convective flux. We estimate that for the experimental systems under consideration, the ratio of convective timescale to diffusion timescale is very small ($\sim 10^{-3}$), making this a reasonable assumption.[38] Calculation of the Péclet numbers are given in the SI. Finally and most importantly, we use the inlet gas flow rate as the effective constant volumetric flow rate in Eqn. (1). While the focus of this paper is vapor fed reactors, this assumption allows for the model to be extended to liquid fed reactors. One issue with this assumption is that various features of the gas channel (e.g., turnaround points) could lead to errors in the assumption of Darcy-like flow due to inertial effects.[40, 41] Another issue is that one would not necessarily expect the volumetric flow rate along the length of the channel to be uniform considering that there can be substantial perturbations to the gas concentration as CO_2 is depleted and water, reaction products, and possibly external sources of gas emerge to contribute to the total volumetric flow rate.[24, 25] Thus we would expect Eqn. (1) to be most applicable to low CO_2 consumption conditions and where water and product gasses compensate for CO_2 losses in the channel (e.g. CO production). We note that this complex issue has been explored experimentally, [31-34] where for example Ma et al.[32] found that the decrease in outlet flow rate relative to inlet flow rate was ~40% for a 15 ml/min feed at 300 mA/cm^2 in a 1 M KOH Cu-catalyst anion exchange membrane VFR. In such situations, Eqn. (1) may not be appropriate for describing single pass conversion efficiency as a function of flow rate; however, for the cases examined below, we find

that Eqn. (1) parameterizes X_{CO_2} vs. Q remarkably well even at low flow rates and high consumptions. In addition to the prior mentioned factors, another reason for such good agreement could be that most of the CO_2 is consumed near the inlet where the flow rate is closer to the feed flow rate, making the choice of feed flow rate a reasonable approximation for Eqn. (1).

With these assumptions in mind, at low feed volumetric flow rate Eqn. (1) plateaus at the internal conversion efficiency X_{CO_2R} of the reactor, which is a measure of how facile CO_2R is compared to (bi)carbonate formation. In the high flow rate regime, Eqn. (1) follows a horizontally shifted $1/Q$-type dependance (see SI). Additionally, Eqn. (1) contains a mass-transport parameter, k_{MT}, that can be used to assess a reactor's overall CO_2 mass-transport characteristics. This parameter is related to both the CO_2R partial current density and (bi)carbonate formation and is thus expected to be strongly dependent on applied voltage, pH in the catalyst layer, CO_2 transport distances, and other reactor characteristics. Notably, for the case of measuring X_{CO_2} vs. Q at constant current instead of constant voltage, which is the situation for all experimental data below, one would expect that k_{MT} would also be a function of the volumetric flow rate of CO_2. In such a case, Eqn. (1) is further simplified to

$$X_{CO_2} = \frac{A_{cat}\left(J_{e,tot} - J_{HER}\right)}{\overline{n}Fc_{CO_2,feed}Q} \tag{2}$$

where $J_{e,tot}$ is the local total electric current density (mA/cm^2), $\overline{n}$ is the average number of electrons per CO_2 molecule reduced, J_{HER} is the total hydrogen evolution current density, and F is Faraday's constant. We present a detailed derivation and discussion of Eqn. (2) in the SI. Thus, if only k_{MT} changes to keep the total current density constant as a function of flow rate, then Eqn. (2) predicts that the single-pass conversion efficiency should scale as $1/Q$ and be directly proportional

to the total applied current density. We note that Eqn. (2) is consistent with the predictions made by substantially more comprehensive 1-D and 2-D models which calculated that at constant flow rate CO_2 conversion scales linearly with total current density over a wide range of applied currents.[24, 26]

As will be demonstrated below, we unexpectedly find that Eqn. (1) parameterizes the data substantially more accurately than Eqn. (2) in the results analyzed. We suspect that a reason for this discrepancy is due to current-compensating effects related to the hydrogen evolution current and possibly the average number of electrons per CO_2 reduced $\overline{n}$ (i.e., the CO_2R product distribution).[28, 35] These changes can alleviate the need for k_{MT} to increase with decreasing flow rate so as to keep the total current density constant. This has been directly observed in experimental data where, for example, O'Brien et al.[28] noted little change in applied voltage as a function of flow rate at a constant 150 mA/cm^2. A more comprehensive model than that used here is needed to understand why literature data appears to follow Eqn. (1) and not Eqn. (2). We make some progress along these lines by verifying that measured k_{MT} values are consistent with those predicted from the model presented by Weng et al.[25] First, however, we demonstrate the fit of Eqn. (1) to multiple sets of experimentally measured single-pass conversion data from different groups.

We begin by applying Eqn. (1) to our own previously published data (**Fig. 2**).

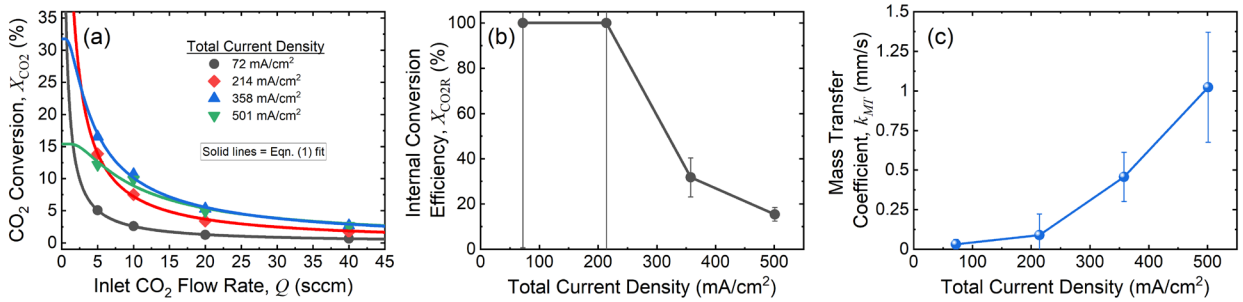

Fig. 2 (a) Application of Eqn. (1) to CO_2 conversion data from Corral et al.[36] (b) The internal conversion efficiency and (c) the overall effective mass transfer coefficients resulting from the fits in (a) as a function of current density. Error bars are 95% confidence intervals of the fit parameter.

Fig. 2a shows that Eqn. (1) describes all single-pass conversion efficiency data presented by Corral et al.[36] across the full measured range of inlet gas flow rates and applied current densities. The resulting internal conversion efficiency and overall mass-transfer coefficient are plotted in **Fig. 2b** and **Fig. 2c**, respectively. For the current density curves in **Fig. 2a** below 250 mA/cm^2, the data do not extend low enough in flow rate to make an accurate determination of internal conversion efficiency (i.e. a wide range of X_{CO_2R} values makes little impact on the sum of squares error), which is why there is significant uncertainty in X_{CO_2R} in that regime of applied current density. Nevertheless, all of the data is captured to a high degree of accuracy by Eqn. (1) using the fit parameters in **Fig. 2b** and **Fig. 2c**.

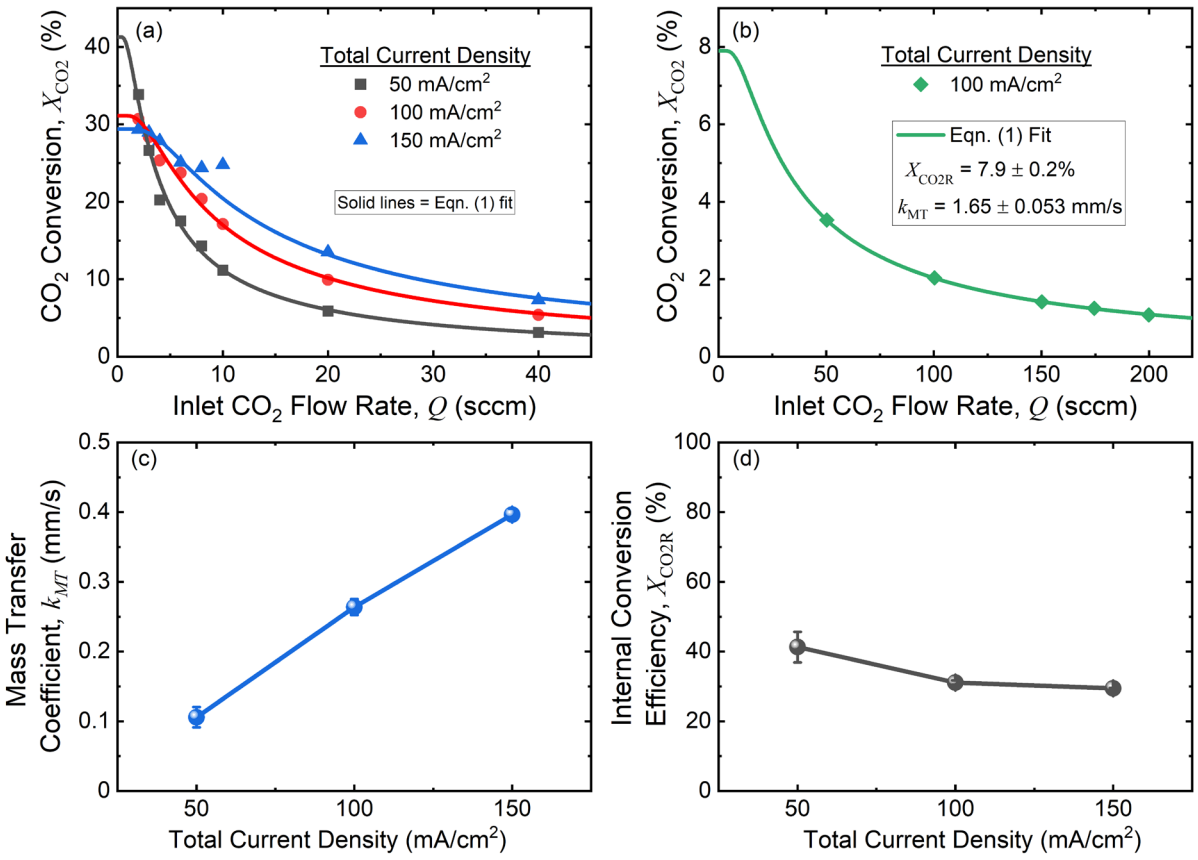

Fig. 3 (a) Application of Eqn. (1) to CO_2 conversion data from Gabardo et al.[35] (b) Application of Eqn. (1) to CO_2 conversion data from Wheeler et al.[37] assuming that A_{cat} = 3 cm^2 in order to calculate k_{MT}. (c) The internal conversion efficiency and (d) the overall effective mass transfer coefficients resulting from the fits in (a) as a function of current density for Gabardo et al.[35] assuming A_{cat} = 5 cm^2. Error bars are 95% confidence intervals of the fit parameter.

To show that Eqn. (1) is generally applicable to a diversity of CO_2 electrolyzers, we also applied our model to the results of Gabardo et al.[35] (**Fig. 3a,c,d**) and Wheeler et al.[37] (**Fig. 3b**). The results of this assessment in **Fig. 3** demonstrate again that Eqn. (1) is able to accurately parameterize single-pass conversion-efficiency data as a function of inlet flow rate over a wide range of flow and current density. The results in **Fig. 3a** in particular are interesting because CO_2 conversion for Gabardo et al.[35] was measured down to inlet flow rates of < 5 sccm and yet Eqn. (1) still describes the curves remarkably well over the entire range of flow rates.

Finally, recent work by O'Brien et al.[28] has detailed an innovative approach to reactor design that largely eliminates the (bi)carbonate formation problem.[23] In terms of the model

presented here, this corresponds to an internal conversion efficiency of 100% or $X_{CO_2R} = 1$. Thus, we would expect that the application of Eqn. (1) to conversion efficiency data from O'Brien et

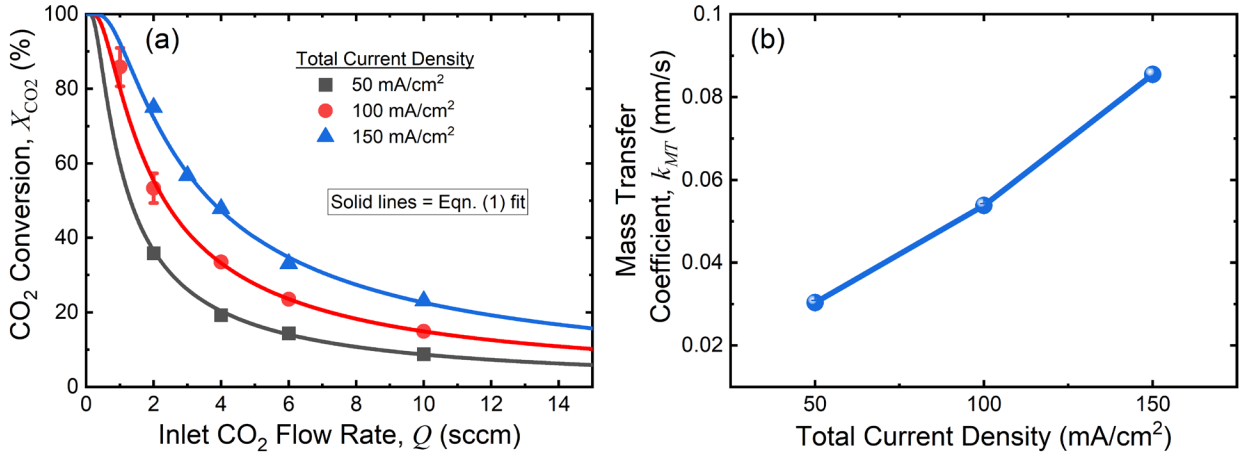

Fig. 4 (a) Application of Eqn. (1) to CO_2 conversion data from O'Brien et al.[28] along with (b) the overall effective mass transfer coefficients resulting from the fits in (a) as a function of current density assuming A_{cat} = 5 cm^2. All curves from Eqn. (1) have $\eta_{ICE} = 1$. The 95% confidence intervals in (b) are smaller than the symbol size.

al.[28] would naturally describe the results with $X_{CO_2R} \approx 1$ across all current densities. **Fig. 4a** shows that this is indeed true, where all three current densities accurately follow Eqn. (1) over all flow rates measured with $X_{CO_2R} = 1$ and k_{MT} values corresponding to **Fig. 4b**. This result further confirms the relevancy of Eqn. (1) by accurately capturing state-of-the-art innovations in reactor design.

In short, **Fig. 2**-**Fig. 4** demonstrate the applicability of the simple descriptive PFR model employed here to capture observed trends in single-pass conversion efficiency as a function of inlet CO_2 flow rate. The excellent goodness of fit (typically $R^2 > 0.999$, Table S1) suggests that the generic rationale is relevant across a diversity of reactor designs made by different research groups. For convenience, we present all the numerical fit parameter results from **Fig. 2**-**Fig. 4** in Table 1 of the SI. With the efficacy of Eqn. (1) demonstrated, we now turn to understanding better

the trends in k_{MT} as function of flow rate and applied current density as shown in **Fig. 2c**, **Fig. 3c**, and **Fig. 4b**.

To gain insight into the extracted k_{MT} parameter in Eqn. (1), we implement the model presented by Weng et al.[25], which can be used to describe CO_2 conversion and consumption from the perspective of a gas-diffusion electrode. This 1D, steady-state model includes the cathode gas-diffusion media and catalyst layer for a silver-catalyst GDE for CO_2 electroreduction with the bulk electrolyte and gas channels as the boundaries. The model is one of the most comprehensive currently published in the literature, and includes key physical phenomena including gas transport, electrochemical reactions using Tafel kinetics, bulk homogenous reactions, diffusion and migration of ions in solution, dissolution of gaseous CO_2 into liquid water, and catalyst-layer saturation (defined as the volume fraction of the layer that is occupied by liquid electrolyte). For simplicity, the modeling results presented here use the exact same equations and parameter set as described in the original manuscript.[25] Importantly, this model does not include a treatment of the gas channel, but rather can be imagined as representing the complex underlying CO_2 sink mechanism beneath a given slice of the gas channel *dx* as shown in **Fig. 1b**. This more comprehensive model can therefore be used to make a better-informed interpretation of experimental k_{MT} values if one makes the same simplifying assumptions about the gas channel as discussed above.

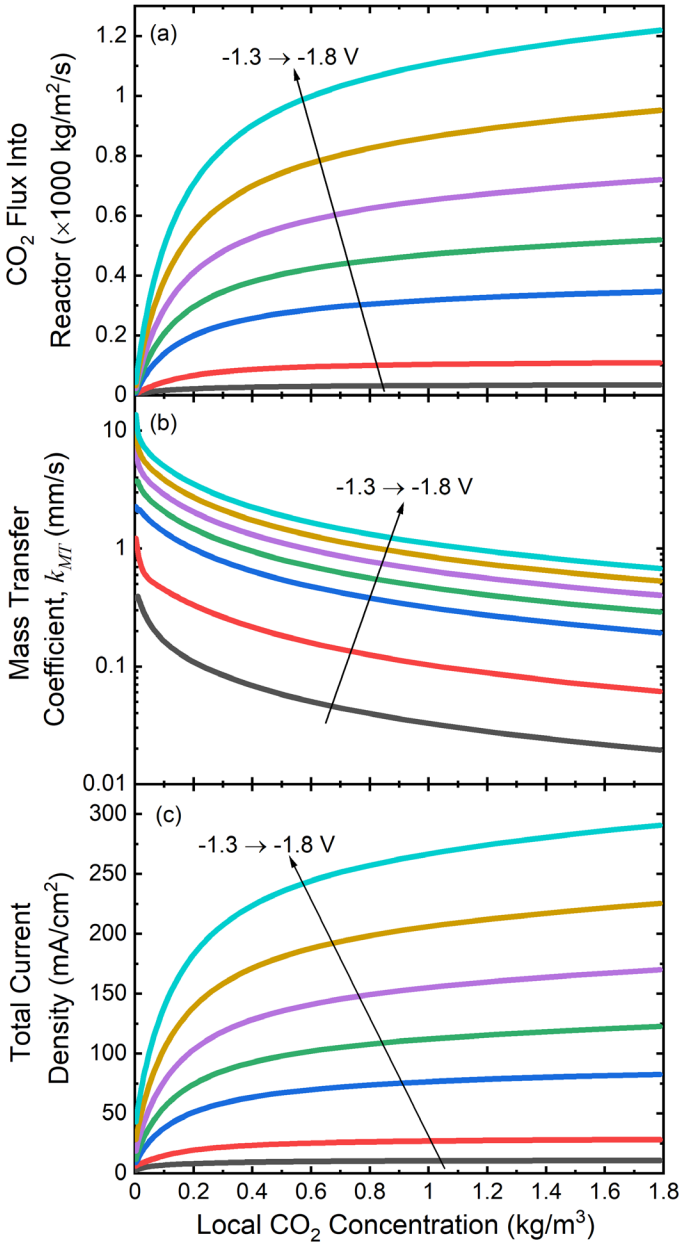

Fig. 5 (a) The calculated local CO_2 flux into a theoretical gas-diffusion electrode, (b) the corresponding effective k_{MT} values from (a) using the definition of Eqn. (S4), and (c) the calculated total current density all as a function of local CO_2 concentration in the gas channel for a series of applied cathodic voltages from -1.3 V to -1.8 V. Note that the voltage steps between curves are not uniform from -1.3 V to -1.8 V.

With this in mind, we begin by examining predictions of k_{MT} as a function of cathodic voltage and local CO_2 concentration in the gas channel. To do so, we fix the mass fraction of $CO_{2(g)}$ over a wide range of values (here 0.02-0.998) and subsequently calculated the steady-state local CO_2 flux and electric current density over a series of applied voltages. For gas transport calculations in

the diffusion medium, we assume that the total mass density is constant and any remaining mass fraction that is not CO_2 is composed of equal mass fractions of CO and H_2. The results of these calculations are shown in **Fig. 5** for a series of applied cathodic potentials from -1.3 V to -1.8 V where the potential is defined in the same manner as in Weng et al.[25] This potential range was chosen to span a range of total current densities that was comparable to the experimental data above. From **Fig. 5a**, we first see that there is a non-linear relationship predicted between the CO_2 flux entering the reactor and the external $CO_{2(g)}$ concentration in the gas channel. Such a dependance directly implies via that k_{MT} is not predicted to be constant as a function of $CO_{2(g)}$ concentration in the gas channel (**Fig. 5b**). However, beyond ~0.8 kg/m^3 (~18 mM) $CO_{2(g)}$, k_{MT} in **Fig. 5b** varies relatively slowly and is reasonably approximated by a constant average value. This high $CO_{2(g)}$ concentration regime is the region where most experiments are conducted and therefore the assumption of constant k_{MT} would be reasonable. Furthermore, these values only represent the conditions at a local slice in the gas channel, whereas experiments represent the average consumption over the entire channel (see SI for calculated internal $CO_{2(g)}$ and electric current density profiles). In any case, it is encouraging that a rough comparison of **Fig. 5b** to values experimentally extracted in **Fig. 2c** and **Fig. 3c** at similar current densities are in reasonable agreement without adjusting any parameters from Weng et al.[25] In terms of the functional dependence of the calculated k_{MT} on CO_2 concentration in the gas channel, we hypothesize that the predicted rise in k_{MT} at lower values of external $CO_{2(g)}$ concentration in **Fig. 5b** is due to increased (bi)carbonate formation caused by an increase in pH at the cathode.[42] In other words, as the $CO_{2(g)}$ supply becomes limited, the pH-decreasing effect of CO_2 dissolution is lessened, which drives up the pH at the cathode and increases (bi)carbonate formation. In terms of our simple model above, this would translate to a non-constant value of X_{CO_2R} as a function of local $CO_{2(g)}$ concentration

that is especially pronounced in strongly CO_2-depleting conditions (i.e., high currents and low flow rates). Finally, similar to our simple PFR model, the model from Weng et al.[25] predicts a significant decrease in electric current density for lower values of the external $CO_{2(g)}$ concentration (**Fig. 5c**). Notably, the total current does not go to zero in **Fig. 5c** when the external $CO_{2(g)}$ is zero due to a finite hydrogen-evolution-reaction (HER) current.[25] As discussed in the SI, this baseline HER current can partly prevent a dramatic drop in total current at low external $CO_{2(g)}$ concentrations (**Fig. S5b**), which we hypothesize is one primary reason why Eqn. (1) is able to describe constant-current experiments. Additionally, the assumption of a constant Tafel slope in the model may not fully capture an increase in HER rate when CO_2 concentrations are low.[43, 44] Additional losses, such as crossover of products and subsequent reaction at the opposite electrode may also contribute to the change in Faradaic efficiencies with potential.

We can further examine what the results of **Fig. 5** imply in terms of the effective measured k_{MT} by numerically solving Eqn. (S1) at numerous voltages for a series of flow rates with $k_{MT}(c_{CO_2})$ interpolated from the relevant curves in **Fig. 5b**. At each flow rate, we can then calculate the total CO_2 consumption and current density by interpolating the relevant values from **Fig. 5** given the final $CO_{2(g)}$ profile from Eqn. (S1). The results of this procedure are shown with open symbols in **Fig. 6a** at currents of 50 mA/cm^2, 100 mA/cm^2, and 150 mA/cm^2. For **Fig. 6a**, we plot the inverse of CO_2 consumption vs. flow rate in order to linearize Eqn. (1) in the high flow rate regime (see Eqn. (S17) in the SI), which allows for direct extraction of k_{MT} from the slope of the line. In **Fig. 6b**, the resulting k_{MT} are values are plotted against current density. Notably, the values of k_{MT} in **Fig. 6b** are in excellent agreement with experimental data in both magnitude and trend with applied total current density. For example, at 150 mA/cm^2 both **Fig. 3c** and **Fig. 6b** both give

$k_{MT} \approx 0.4$ mm/s, which suggests that the order of magnitude of the experimentally extracted k_{MT} values are generally in line with physical expectations as predicted by the model of Weng et al.[25]

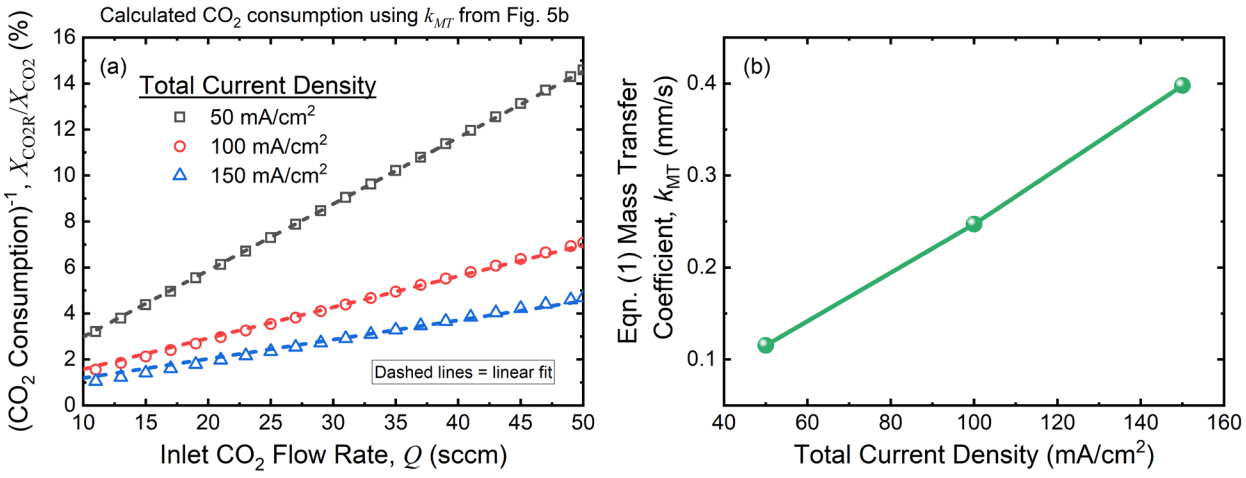

Fig. 6 (a) The inverse of the calculated CO_2 consumption (X_{CO_2R} / X_{CO_2}) using input data from **Fig. 5** for three different current densities along with linear fits. Here we used A_{cat} = 5 cm^2 to align with the experimental data in **Fig. 3**. (b) The corresponding effective k_{MT} values obtained from the slope of the linear fits in (a) from Eqn. (S17).

Now that we have shown Eqn. (1) to be descriptive of experimental data and giving physically reasonable values for the parameters, we turn to one of its key implications for understanding reactor performance. Namely, we use Eqn. (1) to examine the fundamental tradeoff between CO_2 conversion and productivity. Here we define productivity as the amount of CO_2 reduced per unit time normalized to reactor size, where catalyst geometric area A_{cat} is taken as a proxy to represent reactor size. By this definition, productivity and partial CO_2R current density are essentially synonymous. We use CO_2 as opposed to a given product species in this definition to make the analysis more general and easily comparable across reactors; however, one could also easily define productivity on a product basis for more relevance to technoeconomic analysis. With this dimensional definition, one can write an expression for the productivity as

$$\Psi = \frac{c_{CO_2,feed} X_{CO_2} Q}{A_{cat}} \tag{3}$$

where Ψ is the productivity in mol CO_2/s/m^2 or kg CO_2/s/m^2. We can substitute X_{CO_2R} from Eqn. (1) to get

$$\Psi = \frac{c_{CO_2,feed} X_{CO_2R}}{A_{cat}} Q \left(1 - e^{-\frac{k_{MT} A_{cat}}{Q}} \right). \tag{4}$$

For a better sense of productivity trends, it is useful to take the limit of Eqn. (4) as $Q \to \infty$, which results in an expression for maximum productivity

$$\Psi_{\max} = c_{CO_2,feed} X_{CO_2R} k_{MT} \tag{5}$$

where Ψ_{max} is the maximum achievable productivity of the reactor under the condition of zero single-pass conversion (i.e., differential conditions). In other words, Eqn. (5) can be imagined as the limit of what the reactor can consume when the CO_2 concentration in the gas channel is fixed everywhere at $c_{CO_2,feed}$ due to, for example, an extremely high flow rate. Thus, Eqn. (4) can be re-written using Eqn. (5) as

$$\frac{\Psi}{\Psi_{\max}} = \frac{Q}{k_{MT} A_{cat}} \left(1 - e^{-\frac{k_{MT} A_{cat}}{Q}} \right). \tag{6}$$

Inspection of Eqn. (1) and Eqn. (6) indicates that both functions can be plotted in one dimension in terms of the Damköhler number $k_{MT} A_{cat} / Q$. Along these lines, **Fig. 7a** illustrates the

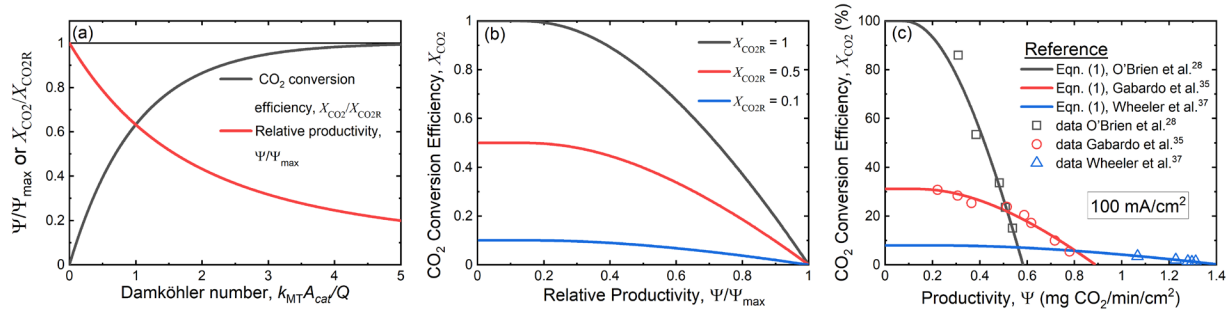

Fig. 7 (a) Single-pass conversion efficiency and relative productivity as a function of the Damköhler number $k_{MT}A_{cat}/Q$. (b) Parametric plot illustrating the tradeoff between conversion efficiency and productivity at different values of X_{CO_2R}. (c) Single-pass conversion efficiency vs. total productivity using parameters from the different references above at a total current density of 100 mA/cm^2. We used $c_{CO_2,feed} = 41$ mM to calculate all curves in (c).

general productivity and conversion curves, giving a sense of the fundamentally opposite trajectories when varying the feed gas flow rate. To illustrate this relationship more directly, **Fig. 7b** shows a parametric plot where productivity is directly plotted against conversion efficiency for all values of Da. The parametric relationship is represented analytically by combining Eqn. (1) and Eqn. (6) to yield

$$\frac{\Psi}{\Psi_{\max}} = -\frac{X_{CO_2} / X_{CO_2R}}{\ln\left(1 - \dfrac{X_{CO_2}}{X_{CO_2R}}\right)}, \tag{7}$$

which is the underlying function for the curves shown in **Fig. 7b**. Eqn. (7) is an important result because it better defines the meaning of reactor performance. For example, it is not relevant to discuss single-pass conversion efficiency or productivity independently without mention of the other because these two KPIs tradeoff against each other when varying the feed flow rate. For a sense of how this analysis practically translates to the data analyzed in this work, we plot in **Fig. 7c** the full dimensional parametric plots of single-pass conversion vs. productivity derived from the parameters of three different studies at an applied total current density of 100 mA/cm^2. The productivity-conversion KPI curves in **Fig. 7c** help one understand the relative merits of each

electrolyzer in a broader sense. For example, the innovation of O'Brien et al.[28] gives access to a wide range of single-pass conversion efficiencies that are not accessible by the other reactors at any flow rate. In the productivity range of ~0.5-0.8 mg CO_2/min/cm^2, however, the reactor presented by Gabardo et al.[35] has the highest CO_2 conversion efficiency but with an overall value less than 25%. Finally, if sub-10% single-pass conversion efficiencies can be tolerated, the work of Wheeler et al.[37] demonstrates excellent performance by being the only device that can reduce > ~0.9 mg CO_2/min/cm^2. The upper limit for productivity at 100 mA/cm^2 with a 2-electron reaction is 1.37 mg CO_2/min/cm^2, which puts Wheeler et al.[37] near the productivity maximum in the high flow rate limit. Notably, we ignore energy consumption here, which would be another factor to consider when assessing the "highest performing" results. In the end, the relative value of conversion efficiency, productivity, and energy consumption must be weighed in economic terms within the context of the application.[12, 15, 16, 20, 45] In our view, though, tradeoff curves like those illustrated in **Fig. 7** can paint a more complete picture of electrolyzer performance and serve as essential inputs to technoeconomic models.[16, 17, 19, 20]

In summary, we derive a simple expression for CO_2 single-pass conversion efficiency and show that it accurately parameterizes the results from a range of experiments from several different research groups. We further demonstrate that the parameters derived from fitting this equation to experimental data are generally consistent with a more comprehensive state-of-the-art model of gas diffusion electrodes that is well accepted in the literature. With the validity of the approach established, we explore the implications for the tradeoff between reactor productivity and single-pass conversion efficiency. Using this approach, researchers can fit their experimental measurements of single-pass conversion efficiency to generate a tradeoff curve for these two KPIs that will allow them to understand the relative merits of their reactor design. Understanding such

relationships are essential for guiding electrolyzer design and operation for turning CO_2 into value-added products.

ASSOCIATED CONTENT

Supporting Information. A brief statement in non-sentence format listing the contents of material supplied as Supporting Information should be included. A listing of the contents of each file supplied as Supporting Information should be included.

ACKNOWLEDGMENT

This work was performed under the auspices of the U.S. Department of Energy by Lawrence Livermore National Laboratory under Contract DE-AC52-07NA27344 and was supported by Laboratory Directed Research and Development funding under project 19-SI-005 and a cooperative research and development agreement among Lawrence Livermore National Laboratory, Stanford University and TOTAL American Services, Inc. (affiliate of TOTAL SE) under agreement number TC02307, which also supported research efforts at Stanford and SLAC National Accelerator Laboratory.

REFERENCES

(1) Qiao, J.; Liu, Y.; Hong, F.; Zhang, J. A review of catalysts for the electroreduction of carbon dioxide to produce low-carbon fuels. *Chem. Soc. Rev.* **2014**, *43*, 631-675. DOI: 10.1039/C3CS60323G.

(2) Jhong, H. R.; Ma, S. C.; Kenis, P. J. A. Electrochemical conversion of CO2 to useful chemicals: current status, remaining challenges, and future opportunities. *Current Opinion in Chemical Engineering* **2013**, *2* (2), 191-199. DOI: 10.1016/j.coche.2013.03.005.

(3) Whipple, D. T.; Kenis, P. J. A. Prospects of CO2Utilization via Direct Heterogeneous Electrochemical Reduction. *The Journal of Physical Chemistry Letters* **2010**, *1* (24), 3451-3458. DOI: 10.1021/jz1012627.

(4) De Luna, P.; Hahn, C.; Higgins, D.; Jaffer, S. A.; Jaramillo, T. F.; Sargent, E. H. What would it take for renewably powered electrosynthesis to displace petrochemical processes? *Science* **2019**, *364* (6438). DOI: 10.1126/science.aav3506.
(5) Higgins, D.; Hahn, C.; Xiang, C.; Jaramillo, T. F.; Weber, A. Z. Gas-Diffusion Electrodes for Carbon Dioxide Reduction: A New Paradigm. *ACS Energy Letters* **2018**, *4* (1), 317-324. DOI: 10.1021/acsenergylett.8b02035.
(6) Clark, E. L.; Resasco, J.; Landers, A.; Lin, J.; Chung, L. T.; Walton, A.; Hahn, C.; Jaramillo, T. F.; Bell, A. T. Standards and Protocols for Data Acquisition and Reporting for Studies of the Electrochemical Reduction of Carbon Dioxide. *Acs Catalysis* **2018**, *8* (7), 6560-6570. DOI: 10.1021/acscatal.8b01340.
(7) Bushuyev, O. S.; De Luna, P.; Dinh, C. T.; Tao, L.; Saur, G.; van de Lagemaat, J.; Kelley, S. O.; Sargent, E. H. What Should We Make with CO2 and How Can We Make It? *Joule* **2018**, *2* (5), 825-832. DOI: 10.1016/j.joule.2017.09.003.
(8) Dinh, C.-T.; Burdyny, T.; Kibria, M. G.; Seifitokaldani, A.; Gabardo, C. M.; García de Arquer, F. P.; Kiani, A.; Edwards, J. P.; De Luna, P.; Bushuyev, O. S.; et al. CO 2 electroreduction to ethylene via hydroxide-mediated copper catalysis at an abrupt interface. *Science* **2018**, *360*, 783-787. DOI: 10.1126/science.aas9100.
(9) Burdyny, T.; Smith, W. A. CO2 reduction on gas-diffusion electrodes and why catalytic performance must be assessed at commercially-relevant conditions. *Energy & Environmental Science* **2019**, *12* (5), 1442-1453. DOI: 10.1039/c8ee03134g.
(10) Kibria, M. G.; Edwards, J. P.; Gabardo, C. M.; Dinh, C. T.; Seifitokaldani, A.; Sinton, D.; Sargent, E. H. Electrochemical CO2 Reduction into Chemical Feedstocks: From Mechanistic Electrocatalysis Models to System Design. *Adv. Mater.* **2019**, *31* (31), e1807166. DOI: 10.1002/adma.201807166.
(11) Garcia de Arquer, F. P.; Dinh, C. T.; Ozden, A.; Wicks, J.; McCallum, C.; Kirmani, A. R.; Nam, D. H.; Gabardo, C.; Seifitokaldani, A.; Wang, X.; et al. CO2 electrolysis to multicarbon products at activities greater than 1 A cm(-2). *Science* **2020**, *367* (6478), 661-666. DOI: 10.1126/science.aay4217.
(12) Grim, R. G.; Huang, Z.; Guarnieri, M. T.; Ferrell, J. R.; Tao, L.; Schaidle, J. A. Transforming the carbon economy: challenges and opportunities in the convergence of low-cost electricity and reductive CO2 utilization. *Energy & Environmental Science* **2020**, *13* (2), 472-494. DOI: 10.1039/c9ee02410g.
(13) Huang, J. E.; Li, F.; Ozden, A.; Sedighian Rasouli, A.; Garcia de Arquer, F. P.; Liu, S.; Zhang, S.; Luo, M.; Wang, X.; Lum, Y.; et al. CO2 electrolysis to multicarbon products in strong acid. *Science* **2021**, *372* (6546), 1074-1078. DOI: 10.1126/science.abg6582.
(14) Wood, J. C.; Grove, J.; Marcellin, E.; Heffernan, J. K.; Hu, S.; Yuan, Z.; Virdis, B. Strategies to improve viability of a circular carbon bioeconomy-A techno-economic review of microbial electrosynthesis and gas fermentation. *Water Res.* **2021**, *201*, 117306. DOI: 10.1016/j.watres.2021.117306.
(15) Welch, A. J.; Digdaya, I. A.; Kent, R.; Ghougassian, P.; Atwater, H. A.; Xiang, C. X. Comparative Technoeconomic Analysis of Renewable Generation of Methane Using Sunlight, Water, and Carbon Dioxide. *Acs Energy Letters* **2021**, *6* (4), 1540-1549. DOI: 10.1021/acsenergylett.1c00174.
(16) Li, W.; Feaster, J. T.; Akhade, S. A.; Davis, J. T.; Wong, A. A.; Beck, V. A.; Varley, J. B.; Hawks, S. A.; Stadermann, M.; Hahn, C.; et al. Comparative Techno-Economic and Life Cycle Analysis of Water Oxidation and Hydrogen Oxidation at the Anode in a CO2 Electrolysis to

Ethylene System. *ACS Sustainable Chemistry & Engineering* **2021**, *9* (44), 14678-14689. DOI: 10.1021/acssuschemeng.1c01846.
(17) Orella, M. J.; Brown, S. M.; Leonard, M. E.; Roman-Leshkov, Y.; Brushett, F. R. A General Technoeconomic Model for Evaluating Emerging Electrolytic Processes. *Energy Technology* **2020**, *8* (11). DOI: ARTN 1900994

10.1002/ente.201900994.
(18) Ramdin, M.; Morrison, A. R. T.; de Groen, M.; van Haperen, R.; de Kler, R.; Irtem, E.; Laitinen, A. T.; van den Broeke, L. J. P.; Breugelmans, T.; Trusler, J. P. M.; et al. High-Pressure Electrochemical Reduction of CO2 to Formic Acid/Formate: Effect of pH on the Downstream Separation Process and Economics. *Industrial & Engineering Chemistry Research* **2019**, *58* (51), 22718-22740. DOI: 10.1021/acs.iecr.9b03970.
(19) Jouny, M.; Luc, W.; Jiao, F. General Techno-Economic Analysis of CO2 Electrolysis Systems. *Industrial & Engineering Chemistry Research* **2018**, *57* (6), 2165-2177. DOI: 10.1021/acs.iecr.7b03514.
(20) Verma, S.; Kim, B.; Jhong, H. R.; Ma, S.; Kenis, P. J. A Gross-Margin Model for Defining Technoeconomic Benchmarks in the Electroreduction of CO2. *ChemSusChem* **2016**, *9* (15), 1972-1979. DOI: 10.1002/cssc.201600394.
(21) Küngas, R. Review—Electrochemical CO2 Reduction for CO Production: Comparison of Low- and High-Temperature Electrolysis Technologies. *J. Electrochem. Soc.* **2020**, *167* (4). DOI: 10.1149/1945-7111/ab7099.
(22) Pant, L. M.; Yang, Z. W.; Perry, M. L.; Weber, A. Z. Development of a Simple and Rapid Diagnostic Method for Polymer-Electrolyte Fuel Cells. *J. Electrochem. Soc.* **2018**, *165* (6), F3007-F3014. DOI: 10.1149/2.0011806jes.
(23) Rabinowitz, J. A.; Kanan, M. W. The future of low-temperature carbon dioxide electrolysis depends on solving one basic problem. *Nat Commun* **2020**, *11* (1), 5231. DOI: 10.1038/s41467-020-19135-8.
(24) Weng, L. C.; Bell, A. T.; Weber, A. Z. Towards membrane-electrode assembly systems for CO2 reduction: a modeling study. *Energy & Environmental Science* **2019**, *12* (6), 1950-1968. DOI: 10.1039/c9ee00909d.
(25) Weng, L. C.; Bell, A. T.; Weber, A. Z. Modeling gas-diffusion electrodes for CO2 reduction. *Phys. Chem. Chem. Phys.* **2018**, *20* (25), 16973-16984. DOI: 10.1039/c8cp01319e.
(26) Kas, R.; Star, A. G.; Yang, K. L.; Van Cleve, T.; Neyerlin, K. C.; Smith, W. A. Along the Channel Gradients Impact on the Spatioactivity of Gas Diffusion Electrodes at High Conversions during CO2 Electroreduction. *Acs Sustainable Chemistry & Engineering* **2021**, *9* (3), 1286-1296. DOI: 10.1021/acssuschemeng.0c07694.
(27) Ripatti, D. S.; Veltman, T. R.; Kanan, M. W. Carbon Monoxide Gas Diffusion Electrolysis that Produces Concentrated C2 Products with High Single-Pass Conversion. *Joule* **2019**, *3* (1), 240-256. DOI: 10.1016/j.joule.2018.10.007.
(28) O'Brien, C. P.; Miao, R. K.; Liu, S.; Xu, Y.; Lee, G.; Robb, A.; Huang, J. E.; Xie, K.; Bertens, K.; Gabardo, C. M.; et al. Single Pass CO2 Conversion Exceeding 85% in the Electrosynthesis of Multicarbon Products via Local CO2 Regeneration. *ACS Energy Letters* **2021**, *6* (8), 2952-2959. DOI: 10.1021/acsenergylett.1c01122.
(29) Jeng, E.; Jiao, F. Investigation of CO2 single-pass conversion in a flow electrolyzer. *Reaction Chemistry & Engineering* **2020**, *5* (9), 1768-1775. DOI: 10.1039/d0re00261e.
(30) Dinh, C. T.; Li, Y. G. C.; Sargent, E. H. Boosting the Single-Pass Conversion for Renewable Chemical Electrosynthesis. *Joule* **2019**, *3* (1), 13-15. DOI: 10.1016/j.joule.2018.10.021.

(31) Ma, M.; Kim, S.; Chorkendorff, I.; Seger, B. Role of ion-selective membranes in the carbon balance for CO2 electroreduction via gas diffusion electrode reactor designs. *Chem Sci* **2020**, *11* (33), 8854-8861. DOI: 10.1039/d0sc03047c.
(32) Ma, M.; Clark, E. L.; Therkildsen, K. T.; Dalsgaard, S.; Chorkendorff, I.; Seger, B. Insights into the carbon balance for CO2 electroreduction on Cu using gas diffusion electrode reactor designs. *Energy & Environmental Science* **2020**, *13* (3), 977-985. DOI: 10.1039/d0ee00047g.
(33) Larrazabal, G. O.; Strom-Hansen, P.; Heli, J. P.; Zeiter, K.; Therkildsen, K. T.; Chorkendorff, I.; Seger, B. Analysis of Mass Flows and Membrane Cross-over in CO2 Reduction at High Current Densities in an MEA-Type Electrolyzer. *ACS Appl Mater Interfaces* **2019**, *11* (44), 41281-41288. DOI: 10.1021/acsami.9b13081.
(34) Larrazábal, G. O.; Ma, M.; Seger, B. A Comprehensive Approach to Investigate CO2 Reduction Electrocatalysts at High Current Densities. *Accounts of Materials Research* **2021**, *2* (4), 220-229. DOI: 10.1021/accountsmr.1c00004.
(35) Gabardo, C. M.; O'Brien, C. P.; Edwards, J. P.; McCallum, C.; Xu, Y.; Dinh, C. T.; Li, J.; Sargent, E. H.; Sinton, D. Continuous Carbon Dioxide Electroreduction to Concentrated Multi-carbon Products Using a Membrane Electrode Assembly. *Joule* **2019**, *3* (11), 2777-2791. DOI: 10.1016/j.joule.2019.07.021.
(36) Corral, D.; Feaster, J. T.; Sobhani, S.; DeOtte, J. R.; Lee, D. U.; Wong, A. A.; Hamilton, J.; Beck, V. A.; Sarkar, A.; Hahn, C.; et al. Advanced manufacturing for electrosynthesis of fuels and chemicals from CO2. *Energy & Environmental Science* **2021**, *14* (5), 3064-3074. DOI: 10.1039/d0ee03679j.
(37) Wheeler, D. G.; Mowbray, B. A. W.; Reyes, A.; Habibzadeh, F.; He, J. F.; Berlinguette, C. P. Quantification of water transport in a CO2 electrolyzer. *Energy & Environmental Science* **2020**, *13* (12), 5126-5134. DOI: 10.1039/d0ee02219e.
(38) Levenspiel, O. *Chemical reaction engineering*; John Wiley & Sons, 1998.
(39) Fogler, H. S. *Essentials of Chemical Reaction Engineering*; Pearson Education, 2017.
(40) Zhang, X. Y.; Zhang, X.; Taira, H.; Liu, H. T. Error of Darcy's law for serpentine flow fields: Dimensional analysis. *J. Power Sources* **2019**, *412*, 391-397. DOI: 10.1016/j.jpowsour.2018.11.071.
(41) Zhang, X. Y.; Zhang, X.; Taira, H.; Liu, H. T. Error of Darcy's law for serpentine flow fields: An analytical approach. *Int. J. Hydrogen Energy* **2018**, *43* (13), 6686-6695. DOI: 10.1016/j.ijhydene.2018.02.070.
(42) Lamaison, S.; Wakerley, D.; Kracke, F.; Moore, T.; Zhou, L.; Lee, D. U.; Wang, L.; Hubert, M. A.; Aviles Acosta, J. E.; Gregoire, J. M.; et al. Designing a Zn-Ag Catalyst Matrix and Electrolyzer System for CO2 Conversion to CO and Beyond. *Adv. Mater.* **2021**, e2103963. DOI: 10.1002/adma.202103963.
(43) Kuhl, K. P.; Cave, E. R.; Abram, D. N.; Jaramillo, T. F. New insights into the electrochemical reduction of carbon dioxide on metallic copper surfaces. *Energy & Environmental Science* **2012**, *5*, 7050. DOI: 10.1039/c2ee21234j.
(44) Hatsukade, T.; Kuhl, K. P.; Cave, E. R.; Abram, D. N.; Jaramillo, T. F. Insights into the electrocatalytic reduction of CO2 on metallic silver surfaces. *Phys. Chem. Chem. Phys.* **2014**, *16*, 13814-13819. DOI: 10.1039/C4CP00692E.
(45) Welch, A. J.; Dunn, E.; DuChene, J. S.; Atwater, H. A. Bicarbonate or Carbonate Processes for Coupling Carbon Dioxide Capture and Electrochemical Conversion. *Acs Energy Letters* **2020**, *5* (3), 940-945. DOI: 10.1021/acsenergylett.0c00234.